Estimation of crystallite size, density, and compositional of the Ti: Al₂O₃ single crystal

Hamdan Hadi Kusuma[1*], Zuhairi Ibrahim[2] and Zulkafli Othaman[3]

[1,2] Physics Department, Faculty of Science and Technology, Universitas Islam Negeri Walisongo Semarang, Central Java, Indonesia
[3] Physics Department, Faculty of Science, Universiti Teknologi Malaysia, Johor Bahru, Malaysia

Corresponding Address: hamdanhk@walisongo.ac.id

ABSTRACT

The purposes of this research were to estimate the crystallite size, density, and chemical composition of the ingot Ti: Al₂O₃ crystal grown by the Czochralski method. The crystallite size and composition of Ti: Al₂O₃ crystals had been determined using x-ray diffraction (XRD) and energy-dispersive x-ray spectroscopy (EDXS). Based on the Archimedes principle, the density of the crystals had been determined. The XRD patterns showed a single central peak with high intensity for all samples. It indicated that all samples had a single crystal. The average value of the samples' crystallite size was in the range of 20.798 nm to 34.294 nm. The ingot crystal density and Ti composition increased from the top to the bottom part because the solid solution was distributed unevenly during the growth process.

INTRODUCTION

Titanium-doped sapphire (Ti: Al₂O₃) is an excellent laser material (Nehari et al., 2011; Sawada et al., 2017). It is the most widely used crystal for wavelength-tunable laser (Panahi et al., 2015; Wu et al., 2020), and it is a leading material in the field of femtosecond pulse lasers (Kozlov & Samartsev, 2013). The Ti: Al₂O₃ single crystal with high quality and uniform dopant distribution can be produced as a high-power tunable laser with a range of wavelengths around ~600nm to ~1100nm (Raeder et al., 2020; Sawada et al., 2017; Zong et al., 2019). A high-quality crystal is required for a tunable solid-state laser.

Single crystal with good characteristics such as high homogeneities and large dimensions can be used on high power laser applications. Its properties affect the compactness of the laser system (Li et al., 2014; Zhou et al., 2015). The quality of the crystal can be improved by knowledge of the growth process's growth parameters and phenomena (Alombert-Goget et al., 2016). A single crystal of Ti: Al₂O₃ can be grown by several methods, i.e., Verneuil method (Alombert-Goget et al., 2016), kyropoulos (Ky) method (Chen et al., 2012; Gao et al., 2015; Nehari et al., 2011; Sen et al., 2020; Stelian et al., 2016; Stelian et al., 2017), temperature gradient technique (TGT) (Ren et al., 2016; Zhou et al., 2006), heat exchange method (HEM) (Dong & Deng, 2004; Joyce & Schmid, 2010), vertical gradient freeze(VGF) method, hydrothermal technique (Song et al., 2005; Wang et al., 2009), micro-pulling down (μ-PD)(Ghezal et al., 2012; Kamada et al., 2018; Zhou et al., 2015), Bridgman method (Han et al., 2020) and Czochralski (Cz) (Alombert-

Goget et al., 2016; Fielitz et al., 2008; Hur et al., 2017; Li et al., 2013, 2014).

Many researchers utilized the grown single crystal from oxide materials as optical and electronic components using the Cz method (Moulton et al., 2019; Spassky et al., 2017). It is because the Cz method can produce high-quality crystals, high homogeneity, and controllable crystal diameter. For the Cz method, a suitable temperature gradient hot zone was required. That means defect can occur during crystal growth into the cooling process when the temperature gradient is more extended (Li et al., 2013, 2014). Knowledge of the growth with the Cz method can produce a single crystal with high homogeneity, high quality, and large dimension. Thereby, a well-controlled single crystal growth process with appropriate growth parameters, including temperature gradients, pull rate, and rotating speed, must be achieved to produce a single crystal with high homogeneity and high quality (Li et al., 2014; Moulton et al., 2019). The crystal's quality is closely related to the transport phenomena and thermal gradient in the furnace (Chen et al., 2014; Hur et al., 2017). So, high-quality and homogeneous crystals can be obtained (Li et al., 2014).

The bubbles formation and their incorporation (Ghezal et al., 2012; Li et al., 2013, 2014) in titanium doped sapphire crystal and the influence of the pulling rate on color center (Alombert-Goget et al., 2016; Li et al., 2014; Zhou et al., 2015) was investigated. The influence of control power on the diameter was studied (Jainal et al., 2010) and the pulling rate on the density and compositional (Kusuma, 2015; Kusuma et al., 2018) of Ti: Al_2O_3 single crystal. This research evaluated the effect of the wafer cut from different positions (top, middle, and bottom) of Ti's ingots: Al_2O_3 with constant pull and rotation rate on the crystallite size, structure, density, and chemical composition.

METHODS

This research employed an experimental method with a quantitative approach. The crystal was grown using the Cz method with Automatic Diameter Control (ADC) System available at Advanced Optical Material Laboratory, Physics Department Universiti Teknologi Malaysia. The characterization of X-ray diffraction (XRD), density, and energy dispersive X-ray spectroscopy (EDXS) were analyzed at Ibnu Sina Institute, Universiti Teknologi Malaysia.

Crystal Growth Process

The raw materials used were polycrystalline with a purity of 99.99% of Ti (0.1 wt. %) doped with Al_2O_3 powders. They were purchased from the Shanghai Institute of Ceramics. The crystal was grown by the Cz method with the ADC system. In the growth process, the iridium crucible with 56.4 mm diameter was inductively heated. The diameter of the crystal can be automatically controlled due to the time derivative of the crystal weight. During the whole crystal growth process, a high vacuum was utilized to avoid oxidation or other crucible damage and crystallization. The Ti: Al_2O_3 crystal was grown with the direction along the c-axis, constant pull rates at 1.50 mmh$^{-1,}$ and rotation rate at and 15 rpm.

Characterization of Ti: Al_2O_3 Crystal

The Ti: Al_2O_3 crystals (top, middle, and bottom part of boule crystal) were analyzed using the XRD, density, and EDXS. XRD analysis was performed to determine the crystal structure and the crystallite size. The crystallite size of the crystal was determined using Debye-Scherrer Equation (1).

$$t = \frac{0.9\lambda}{\beta_{hkl} \cos\theta_{hkl}} \qquad (1)$$

where t is the crystallite size of the crystal, λ is the X-ray source with wavelength 1.540560 nm, β_{hkl} is the full width at half maximum (FWHM), and θ_{hkl} is the angle of diffraction. The density had been calculated

using Equation 2 as a crystal mass (Precisa Model XT 220A) per volume it occupies.

$$\rho = \rho_\ell \frac{W_A}{W_A - W_\ell} \qquad (2)$$

where ρ is the density of crystal, ρ_l is the density of the fluid, W_A is the weight of sample in air, and W_l is the weight in fluid.

The chemical compositional was analyzed using EDXS to identify the elements and concentrations.

RESULTS AND DISCUSSION

Ti crystal: Al_2O_3 was transparent, with no crack and no bubbles (Figure 1). Crystal as wafer was cut with a better mention here of the thickness. For the study, the titanium distribution inside the crystal was chosen three wafers from the top, middle, and bottom (see Figure 1) of the crystal, respectively.
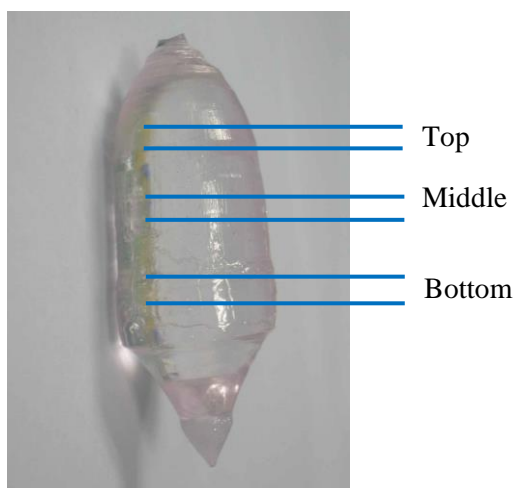

Figure 1. Ti: Al_2O_3 crystal grown Cz method, the crystal was cut from grown along the c-axis.

The structure and crystallite size of Ti: Al_2O_3 crystal can be determined by using X-ray diffraction. All samples have shown a similar diffraction peak. Figure 2 shows that only a single peak was seen and observed for all the samples. It shows that the Ti: Al_2O_3 is a single crystal with relatively good quality. The intensity of the XRD peaks can be affected by many factors related to the crystal morphology composition (Zhang et al., 2020). Figure 2 shows that Ti doping causes the peak to become more intense, and the increase in the relative intensity is proportional to the doping amount. Diffraction peak intensities were decreased when the titanium doped in Al_2O_3 increased. It indicates that the quality of the crystal from top to bottom was decreased. The XRD peaks (see Figure 2) shifted towards the higher angles when titanium doped in Al_2O_3 increased.

The diffraction peak resulted from the XRD pattern was then compared to the Joint Committee on Powder Diffraction Standards (JCPDS) index to determine the diffraction pattern. Therefore, based on the XRD pattern of Ti: Al_2O_3 crystals and JCPDS data (no. 46-1212), The crystal formation of Ti: Al_2O_3 was hexagonal.

Based on the XRD peak of broadening. the crystallite size for Ti: Al_2O_3 crystal was calculated using equation 1. The crystallite size can be estimated using the central peak position (2θ angle) and FWHM of the central peak. The estimated crystallite size of Ti: Al_2O_3 crystals from different positions of the ingot (top, middle, and bottom) are shown in Table 1. It can be seen that the crystallite sizes of Ti: Al_2O_3 single crystal were similar, which suggested the excellent quality single crystal.

Furthermore, the density and chemical composition by EDX analysis can be seen in Tabel 2.
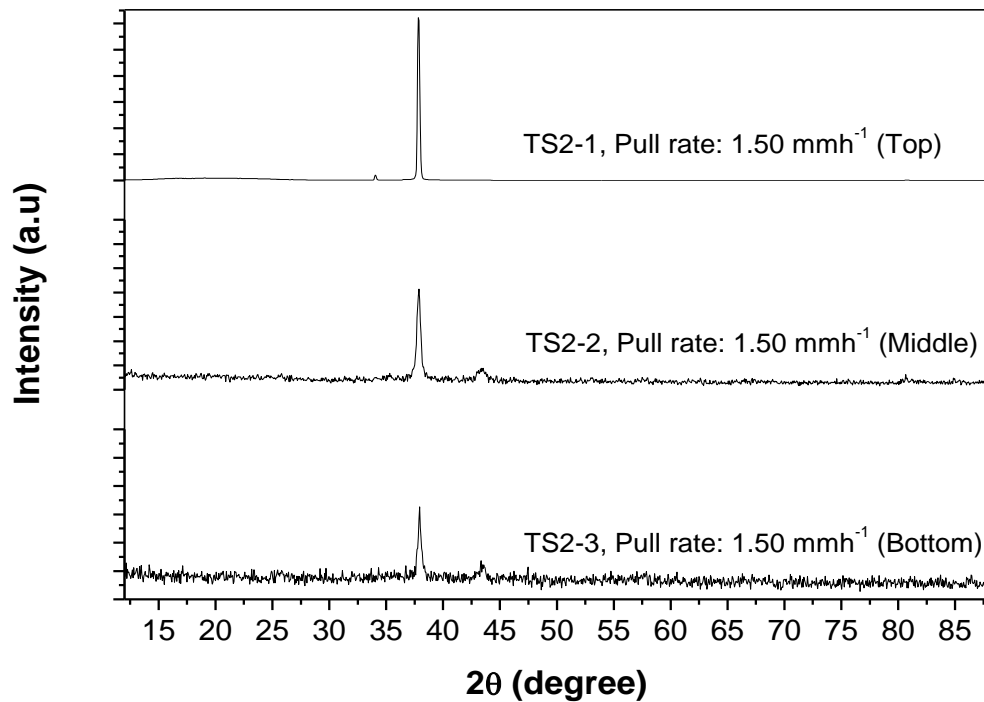
Figure 2. XRD Patterns of Ti (0.1 wt. %): Al_2O_3 Single Crystal With c-cut at a Different Part of the Crystals

Table 1. The estimated crystallite size of Ti: Al_2O_3 single crystal at different position of crystal boules

Samples Name	Dopant (at. %)	2θ (degree)	$d_{(hkl)}$ (Å)	FWHM	t (nm)
TS-1 (top)	0.04	37.839	2.37464	0.245	34.294±0.008
TS-2 (midle)	0.05	37.852	2.37494	0.404	20.798±0.003
TS-3 (bottom)	0.07	37.923	2.37056	0.296	28.392±0.005

Table 2. Result of EDX and the density of Ti (0.1 wt. %): Al_2O_3 crystal at a different part of crystal boules

Sample Name	Pull rate (mmh⁻¹)	Percentage of Atomic (%)				Density (g/cm³)	Remark
		Ti	Al	O	Au		
TS-1	1.5	0.04	56.35	41.82	1.79	3.9946±0.0024	Top
TS-2	1.5	0.05	53.07	45.41	1.47	3.9951±0.0006	Middle
TS-3	1.5	0.07	54.01	43.98	1.95	3.9973±0.0006	Bottom

Based on Table 2, the density of the Ti: Al_2O_3 single crystal from different positions of the ingot (top, middle, and bottom) and the amount of titanium doped in Al_2O_3 had increased. During the crystal growth process, the increase was due to the distribution coefficient and the κ of the solid solution. Therefore, the foreign impurity may easily be trapped and enveloped by the solid phase when the solid-liquid surface advanced slower than mass transport (Chen et al., 2014; Chen et al., 2014; Chen et al., 2012; Kamaruddin et al., 2013; Song et al., 2005). The segregation of Ti atoms was more dominant at the upper than the bottom part of the ingot crystal due to the solid-liquid interface's speed, including the Ti atom, which was faster than that entering into the solid phase. During the growth process, the interface was kept convex so that the entire titanium ions may be rejected to the bottom of the boules. The critical factor affecting the crystals' mechanical and optical properties was the transport of

impurities and dopants in the growth process (Alombert-Goget et al., 2014; Hur et al., 2017). The concentration of dopant had been changing continuously during the growth process.

CONCLUSION AND SUGGESTION

The crystal of Ti: Al_2O_3 was transparent, with no crack and no bubbles. Based on the XRD, it has a single peak, which indicated that it has good quality. The crystallite size of samples was obtained between 20.798 nm to 34.294 nm. The density of the Ti: Al_2O_3 single crystal from different positions of the ingot (top, middle, and bottom) and also the amount of titanium doped in Al_2O_3 were increased.

ACKNOWLEDGMENT

AUTHOR CONTRIBUTIONS

HHK and ZI collected and analyzed data. ZO prepared literature related to research. HHK, ZI and ZO wrote the manuscript.

REFERENCES

Alombert-Goget, G., Lebbou, K., Barthalay, N., Legal, H., & Chériaux, G. (2014). Large Ti-doped sapphire bulk crystal for high power laser applications. *Optical Materials*, *36*(12), 2004–2006. https://doi.org/10.1016/j.optmat.2014.01.011

Alombert-Goget, G., Li, H., Faria, J., Labor, S., Guignier, D., & Lebbou, K. (2016). Titanium distribution in Ti-sapphire single crystals grown by Czochralski and Verneuil technique. *Optical Materials*, *51*(1), 1–4. https://doi.org/10.1016/j.optmat.2015.11.016

Chen, C.-H., Chen, J.-C., Chiue, Y.-S., Chang, C.-H., Liu, C.-M., & Chen, C.-Y. (2014). Thermal and stress distributions in larger sapphire crystals during the cooling process in a Kyropoulos furnace. *Journal of Crystal Growth*, *385*(1), 55–60. https://doi.org/10.1016/j.jcrysgro.2013.04.060

Chen, C., Chen, H. J., Yan, W. B., Min, C. H., Yu, H. Q., Wang, Y. M., Cheng, P., & Liu, C. C. (2014). Effect of crucible shape on heat transport and melt–crystal interface during the Kyropoulos sapphire crystal growth. *Journal of Crystal Growth*, *388*(1), 29–34. https://doi.org/10.1016/j.jcrysgro.2013.11.002

Chen, C. H., Chen, J. C., Lu, C. W., & Liu, C. M. (2012). Effect of power arrangement on the crystal shape during the kyropoulos sapphire crystal growth process. *Journal of Crystal Growth*, *352*(1), 9–15. https://doi.org/10.1016/j.jcrysgro.2012.01.017

Dong, J., & Deng, P. (2004). Ti: sapphire crystal used in ultrafast lasers and amplifiers. *Journal of Crystal Growth*, *261*(4), 514–519. https://doi.org/10.1016/j.jcrysgro.2003.09.049

Fielitz, P., Borchardt, G., Ganschow, S., Bertram, R., & Markwitz, A. (2008). 26Al tracer diffusion in titanium doped single crystalline α-Al2O3. *Solid State Ionics*, *179*(11–12), 373–379. https://doi.org/10.1016/j.ssi.2008.03.007

Gao, Y., Guo, X., & Lu, J. (2015). Analysis of cracking at the bottom during the last stage of kyropoulos sapphire crystal growth【Al2O3】. *International Journal of Science*, *2*(8), 146–153.

Ghezal, E. A., Nehari, A., Lebbou, K., & Duffar, T. (2012). Observation of gas bubble incorporation during micro pulling-down growth of sapphire. *Crystal Growth and Design*, *12*(11), 5715–5719. https://doi.org/10.1021/cg301232r

Han, X., Feng, X., Li, W., & Guo, S. (2020). One kind of new Ti3+ luminous center

in Ti: Al2O3 crystals. *Optical Materials*, *105*(1), 109881. https://doi.org/10.1016/j.optmat.2020.1 09881

Hur, M.-J., Han, X.-F., Choi, H.-G., & Yi, K.-W. (2017). Crystal front shape control by use of an additional heater in a czochralski sapphire single crystal growth system. *Journal of Crystal Growth*, *474*(1), 24–30. https://doi.org/10.1016/j.jcrysgro.2016. 12.078

Jainal, M. N., Ibrahim, Z., & Kusuma, H. H. (2010). Influence of control power on the diameter of Ti: Al2O3 Single Crystal. *Proceedings of 3rd International Conference on Solid State Science & Technology*.

Joyce, D. B., & Schmid, F. (2010). Progress in the growth of large scale Ti: sapphire crystals by the heat exchanger method (HEM) for petawatt class lasers. *Journal of Crystal Growth*, *312*(8), 1138–1141. https://doi.org/10.1016/j.jcrysgro.2009. 11.002

Kamada, K., Murakami, R., Kochurikhin, V. V., Luidmila, G., Jin Kim, K., Shoji, Y., Yamaji, A., Kurosawa, S., Ohashi, Y., Yokota, Y., & Yoshikawa, A. (2018). Single crystal growth of submillimeter diameter sapphire tube by the micro-pulling down method. *Journal of Crystal Growth*, *492*(1), 45–49. https://doi.org/10.1016/j.jcrysgro.2018. 03.023

Kamaruddin, W. H. A., Kusuma, H. H., & Ibrahim, Z. (2013). Effect of new thermal insulation to the growth of LiNbO3 single crystal by czochralski method. *Advanced Materials Research*, *701*, 108–112. https://doi.org/10.4028/www.scientific. net/AMR.701.108

Kozlov, S. A., & Samartsev, V. V. (2013). Femtosecond lasers and laser systems. In *Fundamentals of Femtosecond Optics* (pp. 94–243). Elsevier.

https://doi.org/10.1533/9781782421290 .94

Kusuma, H. H. (2015). X-Ray diffraction and density distribution measurements on the Al2O3 crystals grown by czochralski method with different pull rate. *Journal of Natural Sciences and Mathematics Research*, *1*(1), 1–4. https://doi.org/10.21580/jnsmr.2015.1. 1.475

Kusuma, H. H., Ibrahim, Z., & Othaman, Z. (2018). The density and compositional analysis of titanium doped sapphire single crystal is grown by the Czocharlski method. *Journal of Physics: Conference Series*, *983*(1), 1–7. https://doi.org/10.1088/1742-6596/983/1/012018

Li, H., Ghezal, E. A., Alombert-Goget, G., Breton, G., Ingargiola, J. M., Brenier, A., & Lebbou, K. (2014). Qualitative and quantitative bubbles defects analysis in undoped and Ti-doped sapphire crystals grown by Czochralski technique. *Optical Materials*, *37*(1), 132–138. https://doi.org/10.1016/j.optmat.2014.0 5.012

Li, H., Ghezal, E. A., Nehari, A., Alombert-Goget, G., Brenier, A., & Lebbou, K. (2013). Bubbles defects distribution in sapphire bulk crystals grown by Czochralski technique. *Optical Materials*, *35*(5), 1071–1076. https://doi.org/10.1016/j.optmat.2012.1 2.022

Moulton, P. F., Cederberg, J. G., Stevens, K. T., Foundos, G., Koselja, M., & Preclikova, J. (2019). Characterization of absorption bands in Ti: sapphire crystals. *Optical Materials Express*, *9*(5), 2216–2251. https://doi.org/10.1364/ome.9.002216

Nehari, A., Brenier, A., Panzer, G., Lebbou, K., Godfroy, J., Labor, S., Legal, H., Chériaux, G., Chambaret, J. P., Duffar, T., & Moncorgé, R. (2011). Ti-doped sapphire (Al2O3) single crystals grown by the kyropoulos technique and

optical characterizations. *Crystal Growth and Design*, *11*(2), 445–448. https://doi.org/10.1021/cg101190q

Panahi, O., Nazeri, M., & Tavassoli, S. H. (2015). Design and construction of a tunable pulsed Ti: sapphire laser. *Journal of Theoretical and Applied Physics*, *9*(2), 99–103. https://doi.org/10.1007/s40094-015-0164-x

Raeder, S., Ferrer, R., Granados, C., Huyse, M., Kron, T., Kudryavtsev, Y., Lecesne, N., Piot, J., Romans, J., Savajols, H., Van Duppen, P., & Wendt, K. D. A. (2020). Performance of Dye and Ti: sapphire laser systems for laser ionization and spectroscopy studies at S3. *Nuclear Instruments and Methods in Physics Research Section B: Beam Interactions with Materials and Atoms*, *463*, 86–95. https://doi.org/10.1016/j.nimb.2019.11.024

Ren, Y., Jiao, Y., Vázquez de Aldana, J. R., & Chen, F. (2016). Ti: Sapphire micro-structures by femtosecond laser inscription: Guiding and luminescence properties. *Optical Materials*, *58*, 61–66. https://doi.org/10.1016/j.optmat.2016.05.023

Sawada, R., Tanaka, H., Sugiyama, N., & Kannari, F. (2017). Wavelength-multiplexed pumping with 478- and 520-nm indium gallium nitride laser diodes for Ti: sapphire laser. *Applied Optics*, *56*(6), 1654–1661. https://doi.org/10.1364/AO.56.001654

Sen, G., Alombert Goget, G., Nagirnyi, V., Romet, I., Tran Caliste, T. N., Baruchel, J., Muzy, J., Giroud, L., Lebbou, K., & Duffar, T. (2020). Origin of scattering defect observed in large diameter Ti: Al2O3 crystals grown by the Kyropoulos technique. *Journal of Crystal Growth*, *535*(1), 125530. https://doi.org/10.1016/j.jcrysgro.2020.125530

Song, C., Hang, Y., Xia, C., Zhang, C., Xu, J., & Zhou, W. (2005). Growth of composite sapphire/Ti: sapphire by the hydrothermal method. *Journal of Crystal Growth*, *277*(1–4), 200–204. https://doi.org/10.1016/j.jcrysgro.2004.12.135

Spassky, D. A., Kozlova, N. S., Brik, M. G., Nagirnyi, V., Omelkov, S., Buzanov, O. A., Buryi, M., Laguta, V., Shlegel, V. N., & Ivannikova, N. V. (2017). Luminescent, optical, and electronic properties of Na2Mo2O7 single crystals. *Journal of Luminescence*, *192*, 1264–1272. https://doi.org/10.1016/j.jlumin.2017.09.006

Stelian, C., Sen, G., Barthalay, N., & Duffar, T. (2016). Comparison between numerical modeling and experimental measurements of the interface shape in Kyropoulos growth of Ti-doped sapphire crystals. *Journal of Crystal Growth*, *453*, 90–98. https://doi.org/10.1016/j.jcrysgro.2016.08.001

Stelian, C., Alombert-Goget, G., Sen, G., Barthalay, N., Lebbou, K., & Duffar, T. (2017). Interface effect on titanium distribution during Ti-doped sapphire crystals grown by the Kyropoulos method. *Optical Materials*, *69*, 73–80. https://doi.org/10.1016/j.optmat.2017.04.020

Wang, B., Bliss, D. F., & Callahan, M. J. (2009). Hydrothermal growth of Ti: sapphire (Ti3+: Al2O3) laser crystals. *Journal of Crystal Growth*, *311*(3), 443–447. https://doi.org/10.1016/j.jcrysgro.2008.09.052

Wu, F., Zhang, Z., Yang, X., Hu, J., Ji, P., Gui, J., Wang, C., Chen, J., Peng, Y., Liu, X., Liu, Y., Lu, X., Xu, Y., Leng, Y., Li, R., & Xu, Z. (2020). Performance improvement of a 200TW/1Hz Ti: sapphire laser for laser wakefield electron accelerator. *Optics and Laser Technology*, *131*(June), 1–8.

https://doi.org/10.1016/j.optlastec.2020.106453

Zhang, L., Gonçalves, A. A. S., & Jaroniec, M. (2020). Identification of preferentially exposed crystal facets by X-ray diffraction. *RSC Advances*, *10*(10), 5585–5589. https://doi.org/10.1039/D0RA00769B

Zhou, D., Xia, C., Guyot, Y., Zhong, J., Xu, X., Feng, S., Lu, W., Song, J., & Lebbou, K. (2015). Growth and spectroscopic properties of Ti-doped sapphire single-crystal fibers. *Optical Materials*, *47*, 495–500. https://doi.org/10.1016/j.optmat.2015.06.027

Zhou, G., Dong, Y., Xu, J., Li, H., Si, J.,

Qian, X., & Li, X. (2006). Φ140 mm sapphire crystal growth by temperature gradient techniques and its color centers. *Materials Letters*, *60*(7), 901–904. https://doi.org/10.1016/j.matlet.2005.10.092

Zong, Q.-S., Bian, Q., Xu, C., Chang, J.-Q., He, L.-J., Bo, Y., Zuo, J.-W., Xu, Y.-T., Cui, D.-F., Peng, Q.-J., & Xu, Z.-Y. (2019). High beam quality narrow linewidth microsecond pulse Ti: sapphire laser operating at 819.710 nm. *Optics & Laser Technology*, *113*(November 2018), 52–56. https://doi.org/10.1016/j.optlastec.2018.11.019